An Unsupervised Spatio-Temporal Regularization for Perfusion MRI Deconvolution in Acute Stroke

Mathilde Giacalone, Carole Frindel and David Rousseau*
Université de Lyon, CREATIS ; CNRS UMR5220 ; Inserm U1044 ; INSA-Lyon ;
Université Claude Bernard Lyon 1, France
*E-mail: david.rousseau@creatis.insa-lyon.fr

***Abstract*—We consider the ill-posed inverse problem encountered in perfusion magnetic resonance imaging (MRI) analysis due to the necessity of eliminating, via a deconvolution process, the imprint of the arterial input function on the MR signals. Until recently, this deconvolution process was realized independently voxel by voxel with a sole temporal regularization despite the knowledge that the ischemic lesion in acute stroke can reasonably be considered piecewise continuous. A new promising algorithm incorporating a spatial regularization to avoid spurious spatial artifacts and preserve the shape of the lesion was introduced [1]. So far, the optimization of the spatio-temporal regularization parameters of the deconvolution algorithm was supervised. In this communication, we evaluate the potential of the L-hypersurface method in selecting the spatio-temporal regularization parameters in an unsupervised way and discuss the possibility of automating this method. This is demonstrated quantitatively with an in silico approach using digital phantoms simulated with realistic lesion shapes.**

I. Introduction

Stroke – a neurological deficit resulting from blood supply perturbations in the brain – is a major public health issue, representing the third cause of death in industrialized countries. There is an important need to be able to identify patients eligible to the different therapies and evaluate the benefit-risk ratio for the patients. In this context, Dynamic Susceptibility Contrast (DSC) perfusion MRI is one of the imaging modality used in clinical routine as a diagnostic tool since it allows to compute parameters reflecting the state of perfusion of the cerebral tissues. A DSC-perfusion MRI is a time series of MRI images, the acquisitions of which are synchronized with the intravascular bolus injection of a contrast-agent. The MR signal recorded in each voxel can be used to calculate the concentration-time curve of the contrast-agent in the tissues within each voxel. The shape of each concentration-time curve will not only depend on the state of perfusion of the tissues within the voxel – information of clinical interest – but also on the shape of the contrast-agent bolus at its arrival in the brain, commonly referred to as the arterial input function. However – due, among other things, to the inter-individual variability in cardiac functions – each patient has an unique arterial input function. Consequently, a step of deconvolution is necessary in order to eliminate the contribution of the arterial input function and extract the clinically relevant information.

The contrast-agent concentration can be modeled as the convolution of the arterial input function with an impulse response function which contains the information on the state of perfusion. The deconvolution step corresponds to the computation of this impulse response function from the contrast-agent concentration and the arterial input function, which can both be calculated from the perfusion image. This deconvolution step corresponds to the resolution of an ill-posed inverse problem which requires the use of a priori information, for example the introduction of regularity constraints on the solution. To the best of our knowledge, the deconvolution algorithms currently used in clinical routine only consider the deconvolution of each contrast-agent concentration-time curves independently, ignoring the correlation between neighboring voxels inherent to the structured organization of the brain tissues. Frindel et al. [1] recently proposed a new edge-preserving deconvolution algorithm with a spatio-temporal regularization that exploits the correlation between neighboring voxels. This algorithm was illustrated on synthetic data as well as on real data from a retrospective study and its efficiency and interest was demonstrated for acute stroke after a supervised optimization of the spatio-temporal regularization parameters. However, since the supervised optimization of the parameters is not possible for real data in clinical routine, it is important to be able to optimize these parameters in an unsupervised fashion.

Numerous methods for the unsupervised optimization of regularization parameters have been proposed in the literature, although most are concerned with the optimization of a single regularization parameter [2] and are not always easily extendable to multiple parameters optimization. Amongst them however, the L-curve method [3] was extended to the multi-dimensional case [4] [5]. Although the L-curve method is a fairly popular method in practice for its intuitive principle, simplicity of implementation and because it does not require any a priori knowledge about the noise, its applicability in a specific context needs to be verified on a one to one basis.

In this communication we discuss the possibility of automatically optimizing in an unsupervised manner the spatio-temporal regularization parameters of the deconvolution algorithm proposed by Frindel et al. [1] by using a method generalizing the L-curve method, namely the L-hypersurface method. The communication is organized as follows. We first present the synthetic data which were specifically designed to test the performance of the L-hypersurface method for the optimization of spatio-temporal regularization parameters in application to stroke. We then present the deconvolution

978-0-9928-6265-7/16/$31.00 ©2016 IEEE

algorithm proposed in Frindel et al. [1] as well as an upgraded version of this algorithm containing a new non-negativity constraint. The L-hypersurface method is then explained and its performance is evaluated in our specific framework. Finally, a method for the automation of the L-hypersurface method is proposed and its performance discussed.

II. Synthetic data

In order to evaluate the performance of the L-hypersurface method for the unsupervised optimization of regularization parameters, we need to be able to define a target set of regularization parameters. We therefore chose to work with synthetic data, where the true impulse response function for each voxel is known and where we will be able to calculate objectively the optimal set of regularization parameters. In the treatment of stroke patient images, lesion shape was recently shown to be a biomarker of interest for the prediction of the final volume infarct [6]. We will therefore design images that have realistic lesion shapes, as well as realistic pathological and healthy perfusion values.

The contrast-agent concentration-time images and their corresponding impulse response images are simulated from four 2D label images – extracted from the I-KNOW database [6] – which determine the tissue type of each voxel: healthy tissue, ischemic tissue or background voxels (cf. Fig. 1). The lesion shapes of each label images were chosen specifically to be representative of the variability observed in the I-KNOW database. The contrast-agent concentration associated to each voxel v, $C_v(t)$ (mM), is modeled as the convolution of a global arterial input function, $C_a(t)$ (mM), and an impulse response function specific to each voxel v, $f_v(t)$: $C_v(t) \sim \int_0^t C_a(\tau) f_v(t-\tau) d\tau$, where $C_a(t)$ is a gamma function and $f_v(t) = \text{CBF}_v$ for $t \leq \text{MTT}_v$ and $f_v(t) = 0$ for $t > \text{MTT}_v$, with CBF_v the cerebral blood flow and MTT_v the mean transit time. The impulse response function $f_v(t)$ corresponds to the ground truth after deconvolution of each voxel v and contains the information on the state of perfusion of clinical interest, namely CBF_v and MTT_v. The CBF and MTT are set respectively to 40 mL/100g/min and 4.5 s for healthy tissues and to 10 mL/100g/min and 9 s for ischemic tissues. Background voxels are simply set to 0 for all time points. A Gaussian noise, meant to model the fluctuations in the MRI acquisition system, is finally added to the images in order to obtain a peak signal to noise ratio over the brain voxels of 22.6 dB, typical of the noise level observed in clinical data [1].

The interest of using simulated data is that the quality of the impulse response image obtained after deconvolution can be evaluated quantitatively since the true impulse response image is known. Since the CBF is amongst the perfusion parameters of great clinical interest [7] [8] and can easily be extracted after deconvolution as $\text{CBF}_v = \max(f_v(t))$ for all voxel v, we propose here to use as a quantitative quality criteria the MAPE defined as the mean absolute percentage error value in the brain tissues (ignoring the background voxels) on the CBF map:

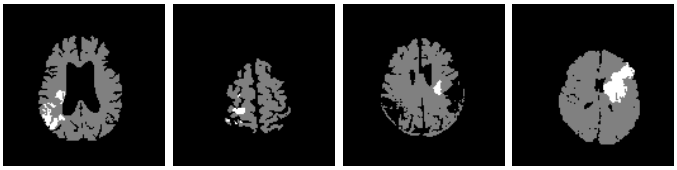

Fig. 1. 2D-label images used for the simulation: in gray, the healthy tissues; in white, the ischemic tissues; in black, the background voxels.

$$\text{MAPE } (\%) = 100 * \frac{1}{N_v} \sum_{v \in \text{brain}} \left| \frac{\widehat{\text{CBF}}_v - \text{CBF}_v}{\text{CBF}_v} \right| , \quad (1)$$

with N_v the number of voxels in the brain, $\widehat{\text{CBF}}_v$ the cerebral blood flow estimated after deconvolution in voxel v and CBF_v the true cerebral blood flow in voxel v. The deconvolution algorithms used in this paper are described in the following section.

III. Deconvolution algorithm

Frindel et al. [1] proposed to address the deconvolution problem with the minimization, over the impulse response image f, of a global cost function Ω composed of a data-fidelity term $\Phi(f)$ and of two a priori terms corresponding to spatial ($\Psi_s(f)$) and temporal ($\Psi_t(f)$) regularization constraints:

$$\Omega(f) = \Phi(f) + \lambda_s \Psi_s(f) + \lambda_t \Psi_t(f) , \quad (2)$$

where λ_s and λ_t are the regularization parameters controlling respectively the strength of the spatial and temporal regularizations. We also propose an upgraded version of this algorithm containing an additional a priori term, a non-negativity constraint, based on the knowledge that an impulse response function is necessarily positive:

$$\Omega(f) = \Phi(f) + \lambda_s \Psi_s(f) + \lambda_t \Psi_t(f) + \lambda_p \|(-f)^+\|_2^2 , \quad (3)$$

with $(-f)^+ = \max(-f, 0)$. The regularization parameter λ_p controlling the strength of the non-negativity constraint is fixed to a high value since the non-negativity constraint is a very strong a priori knowledge. The explicit expressions of $\Phi(f)$, $\Psi_s(f)$ and $\Psi_t(f)$ are detailed in [1].

The solution obtained after deconvolution – that is the impulse response image $f^*_{\mathbf{\Lambda}}$ minimizing Ω for a given set of regularization parameters $\mathbf{\Lambda} = (\lambda_s, \lambda_t)$ – will vary considerably depending on the choice of $\mathbf{\Lambda}$. The good behaviour of the deconvolution algorithms – that is their ability to give a robust solution, close to the true impulse response image – will depend on the appropriate tuning of this set of regularization parameters. Generally, nothing is known of the true impulse response image and we therefore need a method to optimize these regularization parameters in an unsupervised manner. In the following, we evaluate the performance of the unsupervised L-hypersurface method [5] in selecting a good set of regularization parameters for our specific application.

IV. The L-hypersurface method

A. Principle

The L-hypersurface method is a method for the optimization of regularization parameters in global cost functions used for the resolution of ill-posed inverse problems [5]. It generalizes the L-curve method introduced by Hansen [3] for the optimization of a single regularization parameter in ill-posed problems to the optimization of multiple regularization parameters. This method requires the minimization of the cost function associated to the inverse problem of interest (Ω) for a wide range of sets of regularization parameters. For each set of regularization parameters $\mathbf{\Lambda_i}$, a solution $f^*_{\mathbf{\Lambda_i}}$ and its corresponding cost function value $\Omega(f^*_{\mathbf{\Lambda_i}})$ is obtained. Once the screening of the sets of regularization parameters is finished, the (N+1)-dimensional hypersurface corresponding to the plot of the data-fidelity term as a function of the N regularization terms of the global cost function must be displayed. This plot must be drawn in an appropriate scale, generally a decimal logarithm or a square root scale. In our case, the hypersurface corresponds to the plot of the data fidelity term, $\Phi(f^*_{\mathbf{\Lambda_i}})$, as a function of the spatial and temporal regularization terms, $\Psi_s(f^*_{\mathbf{\Lambda_i}})$ and $\Psi_t(f^*_{\mathbf{\Lambda_i}})$, where each point is associated to a given set of regularization parameters $\mathbf{\Lambda_i} = (\lambda_{s_i}, \lambda_{t_i})$.

The shape of the hypersurface obtained will then determine if the L-hypersurface method can be used or not for the given application under consideration. The method can only be used in cases where the hypersurface takes a distinctive bent-shape [5], hence the name of L-hypersurface method. The corner of the bend will be more or less well-defined depending on the scale and particular regularization method used as well as on the difficulty intrinsic to the specific data under consideration. In favourable cases, the upper part of the bend corresponds to solutions that are over-smoothed, with a corresponding cost function which has small regularization terms but a large data-fidelity term. The lower part of the bend corresponds to solutions that are under-smoothed, with a corresponding cost function which has large regularization terms but a small data-fidelity term. The corner of the hypersurface is considered to give the best compromise between a good fit to the data and a reasonably smooth solution. The optimization of a N-dimensional set of regularization parameters with the L-hypersurface method therefore simply consists in selecting the set of regularization parameters $\mathbf{\Lambda}_{\text{corner}}$ associated with the corner of the hypersurface.

B. Performance

In this study, we screened, for each simulation, 1568 sets of regularization parameters $\mathbf{\Lambda}$ with λ_t varying from 10^{-4} to 10^5 and with λ_s varying from 10^{-7} to 10^3. We applied a decimal logarithm transformation and normalized each dimension separately between 0 and 1 before plotting the hypersurface. Note that this results in using a different scale – γ_x, γ_y and γ_z – for each dimension. As illustrated in Fig. 2, the hypersurface obtained presented a clear bent-shape for all simulations (no matter the shape of the 2D-label image used), which ensures that the L-hypersurface method is applicable in our specific context.

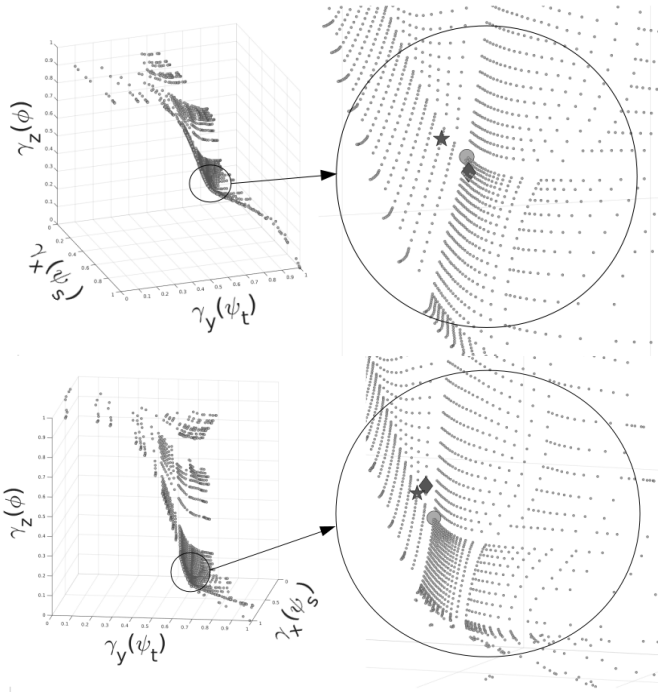

Fig. 2. Global view of the hypersurface and zoom of the corner region. Hypersurface obtained with the synthetic data described in section II when the deconvolution algorithm described in Eq. 2 is used (Top) or when the deconvolution algorithm described in Eq. 3 is used (Bottom). The star corresponds to the optimum, the circle to the true corner of the hypersurface and the diamond to the automatically detected corner.

Now that the applicability of the L-hypersurface method in our specific context has been verified, we need to evaluate the quality of the set of regularization parameters $\mathbf{\Lambda}_{corner}$ chosen by the L-hypersurface method (cf circle in Fig. 2) by comparaison to the true optimal set of regularization parameters $\mathbf{\Lambda}_{optim}$ (cf star in Fig. 2), defined as the set minimizing the MAPE quality criteria (cf Eq. 1). For all simulations, the optimal set of regularization parameters was never exactly positioned in the corner of the L-hypersurface, but always fairly close to it (cf Fig. 2 for illustration). We propose here to use as a quantitative performance indice of the L-hypersurface method for selecting a good set of regularization parameters the indice PI which corresponds to the difference between the quality of the results obtained after deconvolution when using the set of regularization parameters selected with the L-hypersurface method and of the results obtained when using the true optimal set of regularization parameters:

$$\text{PI} = \text{MAPE}_{\Lambda_{corner}} - \text{MAPE}_{\Lambda_{optim}} \ . \tag{4}$$

In order to account for the variability due to noise, we deconvolved 30 different noise realizations (for each label image shown in Fig. 1) with both $\mathbf{\Lambda}_{optim}$ and $\mathbf{\Lambda}_{corner}$ and calculated for each of them the performance indice's value. A summary of the results obtained after deconvolution with the upgraded version of the deconvolution algorithm is given in

TABLE I
MEAN ± SD OF THE PERFORMANCE INDICE (%) DEFINED IN EQ. 4 OBTAINED OVER 30 NOISE REALIZATIONS FOR EACH OF THE DIFFERENT 2D-LABEL IMAGES.

	L1	L2	L3	L4
PI	4.0 ± 0.1	3.2 ± 0.1	3.9 ± 0.2	5.1 ± 0.2

Table I. In average, we found a 4.05 % quality difference between the CBF map obtained after deconvolution with $\mathbf{\Lambda}_{optim}$ and $\mathbf{\Lambda}_{corner}$. This quality drop is reasonable and the L-hypersurface method appears to constitute a very simple and satisfying method for the selection of our regularization parameters. For the results given in Table I however, the hypersurface corner was manually detected based on a visual inspection and we will now address the question of the automatic detection of this corner.

V. AUTOMATION OF THE OPTIMIZATION

A. Automation method

The automation of the corner detection in the L-hypersurface method has been discussed in [5] where they defined the corner as the point closest to a judiciously chosen origin (x_0, y_0, z_0). However, a robust mean of selecting this origin in cases where there is more than one regularization term was not detailed. We propose here a new method for the automatic selection of this origin and hence the automatic detection of the corner. We noticed a considerable difference in the shape of the under-smoothed region between the hypersurface computed after deconvolution with the original algorithm and those computed with the algorithm containing the non-negativity term. In the latter case, the under-smoothed region appears atrophied (cf Fig. 2, bottom). We therefore propose a slight difference in the origin selection method depending on the deconvolution algorithm used. The proposed method is divided into two steps :

1. The first step of our method is to detect the most likely candidates for the corner. i) Initialize the set of corner candidates $\mathcal{S}_{CC}$ to the points which are neither in the highest over-smoothed region (arbitrarily defined as $\mathcal{S}_{\text{over-smoothed}} = \{(x_i, y_i, z_i) | z_i > \frac{75}{100}\}$) nor in the highest under-smoothed region (arbitrarily defined as $\mathcal{S}_{\text{under-smoothed}} = \{(x_i, y_i, z_i) | z_i < \frac{15}{100}\}$). ii) Conduct a principal component analysis on the data points and select between the first and second principal plane, the plane $\mathcal{P}$ closer to the diagonal plane of normal vector [1,1,0] and positioned such that 60% of points are below the plane. Discard from the set of corner candidates $\mathcal{S}_{CC}$ the points that are above the plane. An illustration of this step is given in the upper part of Fig. 3.

2. The second step of our method is then to compute the origin (x_0, y_0, z_0). In order to do so, we will use the points with high z-values to choose x_0 and y_0, and the points with low z-values to choose z_0. Since the hypersurface is sometimes contorted we will also use the principal directions to correct the position of the origin. i) Compute $X_b = (x_b, y_b, z_b)$, the mean coordinates of all the data points having a z-value higher than the maximum z-value of the corner candidates. ii) Compute $X_c = (x_c, y_c, z_c)$, the mean coordinates of all the data points having a z-value lower than the minimum z-value of the corner candidates. iii) Compute $X_{pb} = (x_{pb}, y_{pb}, z_{pb})$ the projection of X_b on the first principal plane passing through X_c (cf Fig. 3, bottom). iv) Compute $X_{pc} = (x_{pc}, y_{pc}, z_{pc})$ the projection of X_c on the first principal plane passing through X_b. v) Set $x_0 = (x_b + x_{pb})/2$, $y_0 = (y_b + y_{pb})/2$ and $z_0 = (z_c + z_{pc})/2$ for the deconvolution algorithm with the non-negativity term or $z_0 = \min(z \in \mathcal{S}_{CC})$ for the deconvolution algorithm without the non-negativity term.

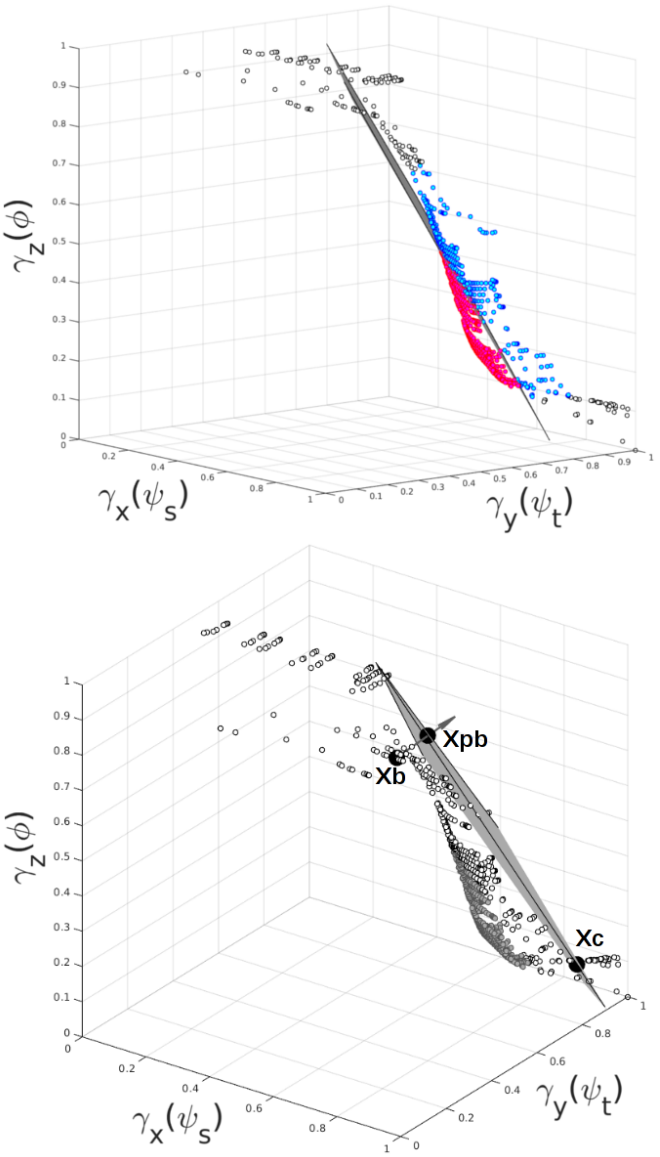

Fig. 3. Illustration of our method for the origin selection. (Top) Illustration of step 1. The points in white correspond to the points in the highest over- or under-smoothed regions. The points in red, below plane $\mathcal{P}$ (in gray), correspond to the set of corner candidates selected at the end of step 1. (Bottom) Illustration of step 2.iii) which corresponds to the projection of X_b on the first principal plane passing through X_c.

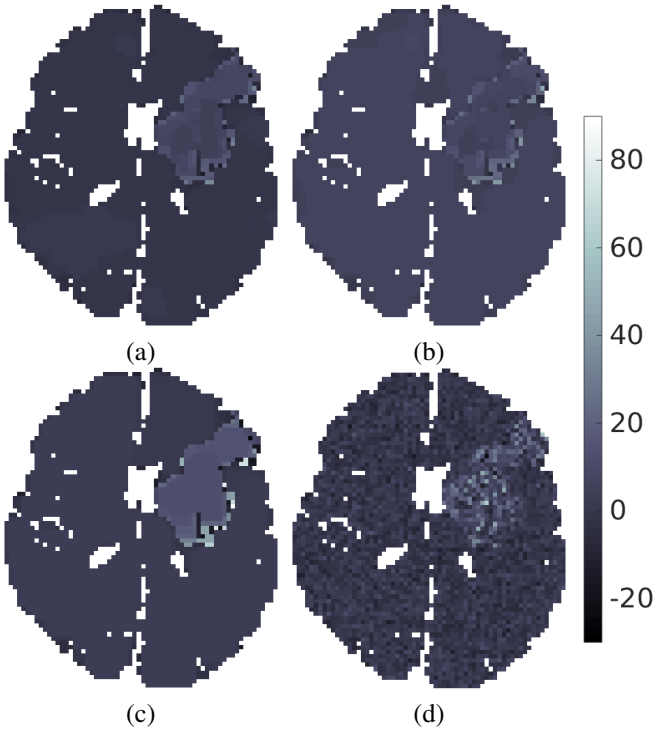

Fig. 4. (a+b+c) Percentage error $100 * \left(\widehat{\text{CBF}_v} - \text{CBF}_v\right) / \text{CBF}_v$ of the CBF value computed after deconvolution with the algorithm described in Eq. 3 , (a) when the optimum set of spatio-temporal regularization parameters is used, (b) when the set corresponding to the true corner of the L-hypersurface is used and (c) when the set corresponding to the automatically detected corner is used. (d) Shows the results obtained when only a temporal regularization term is used in the deconvolution algorithm, which corresponds to one of the most commonly used algorithm for the time being.

B. Performance of the method

Fig. 2 illustrates the performance of our corner detection method. The detected corner, the gray diamond on the figure, seems relatively well positioned, although not exactly on the true corner of the hypersurface. We calculated for all hypersurfaces $RI = \frac{\|X_\diamond - X_\circ\|_2}{\|X_* - X_\circ\|_2}$, the ratio of the distance between the coordinates $X_\circ$ of the true corner of the hypersurface and $X_\diamond$ of the detected corner and the distance between the coordinates $X_\circ$ of the true corner of the hypersurface and the coordinates X_* for the optimal set of regularization parameters. In average we found a value of 0.4 which demonstrates the good performance of our automatic detection method. Fig. 4(a+b+c) illustrates the performance of the deconvolution algorithm presented in Eq. 3 when the different strategies for choosing the regularization parameters are used. Fig. 4(d) shows the result obtained with a deconvolution containing the temporal regularization term only. As one can see, the spurious artifacts present after deconvolution with a temporal regularization only are eliminated after deconvolution with a spatio-temporal regularization.

VI. Conclusion

We have tested the use of the L-hypersurface method, with a new corner detection method, to automatically adjust in an unsupervised manner the spatio-temporal regularization parameters in the deconvolution of DSC-perfusion MRI of acute stroke patients. We evaluated the performance of this method with a numerical simulation approach, allowing a quantitative evaluation of the method. We are currently completing this approach with tests on real data such as those proposed in [1] for clinical prediction outcome [6]. The obtained results demonstrate that the automatically obtained solutions are satisfactorily close to the in-silico ground truths. This constitutes promising results for the dissemination of the new deconvolution algorithm with spatio-temporal regularization proposed by [1] and its upgraded version proposed here, which is known to outperform the techniques currently implemented in clinical imaging platforms which only use a purely temporal regularization. In future research, we believe it would be very interesting to extend our automatic method for the detection of the hypersurface corner by taking into account the information on the hypersurface curvature. The corner corresponds to the point of maximum curvature in a locally convex region [3] and we therefore expect the addition of information on the curvature to improve the performance of our method.

Acknowledgment

This work was supported by the LABEX PRIMES (ANR-11-LABX-0063) of Université de Lyon, within the program "Investissements d'Avenir" (ANR-11-IDEX-0007) operated by the French National Research Agency (ANR).

References

[1] C. Frindel, M. C. Robini, and D. Rousseau, "A 3-D spatio-temporal deconvolution approach for MR perfusion in the brain," *Medical Image Analysis*, vol. 18, no. 1, pp. 144–160, 2014.

[2] F. Bauer and M. A. Lukas, "Comparing parameter choice methods for regularization of ill-posed problems," *Mathematics and Computers in Simulation*, vol. 81, no. 9, pp. 1795–1841, 2011.

[3] P. C. Hansen and D. P. O'Leary, "The use of the l-curve in the regularization of discrete ill-posed problems," *SIAM Journal on Scientific Computing*, vol. 14, no. 6, pp. 1487–1503, 1993.

[4] D. H. Brooks, G. F. Ahmad, R. S. MacLeod, and G. M. Maratos, "Inverse electrocardiography by simultaneous imposition of multiple constraints," *Biomedical Engineering, IEEE Transactions on*, vol. 46, no. 1, pp. 3–18, 1999.

[5] M. Belge, M. E. Kilmer, and E. L. Miller, "Efficient determination of multiple regularization parameters in a generalized L-curve framework," *Inverse Problems*, vol. 18, no. 4, pp. 1161–1183, 2002.

[6] C. Frindel, A. Rouanet, M. Giacalone, T. Cho, L. Østergaard, J. Fiehler, S. Pedraza, J. Baron, M. Wiart, Y. Berthezène, N. Nighoghossian, and D. Rousseau, "Validity of shape as a predictive biomarker of final infarct volume in acute ischemic stroke," *Stroke*, vol. 46, no. 4, pp. 976–981, 2015.

[7] J. Fiehler, M. von Bezold, T. Kucinski, R. Knab, B. Eckert, O. Wittkugel, H. Zeumer, and J. Röther, "Cerebral blood flow predicts lesion growth in acute stroke patients," *Stroke*, vol. 33, no. 10, pp. 2421–2425, 2002.

[8] S. Christensen, K. Mouridsen, O. Wu, N. Hjort, H. Karstoft, G. Thomalla, J. Röther, J. Fiehler, T. Kucinski, and L. Østergaard, "Comparison of 10 perfusion mri parameters in 97 sub-6-hour stroke patients using voxel-based receiver operating characteristics analysis," *Stroke*, vol. 40, no. 6, pp. 2055–2061, 2009.